Traffic 2007
Blackwell Munksgaard

doi: 10.1111/j.1600-0854.2007.00578.x

The Conserved Isoleucine–Valine–Phenylalanine Motif Couples Activation State and Endocytic Functions of β-Arrestins

Anne Burtey[1,2], Eva M. Schmid[3,†], Marijn G. J. Ford[3,†], Joshua Z. Rappoport[4,†], Mark G. H. Scott[1,2,†], Stefano Marullo[1,2], Sanford M. Simon[4], Harvey T. McMahon[3] and Alexandre Benmerah[1,2,*]

[1]Institut Cochin, Université Paris Descartes, CNRS (UMR 8104), Paris, France
[2]INSERM, U567, 75014 Paris, France
[3]MRC Laboratory of Molecular Biology, Cambridge, CB2 2QH, UK
[4]The Laboratory of Cellular Biophysics, The Rockefeller University, New York, NY 10021, USA
**Corresponding author: Alexandre Benmerah, benmerah@cochin.inserm.fr*
†*These authors contributed equally to this work.*

Beta-arrestins (βarrs) play a central role in the regulation of G-protein-coupled receptors (GPCRs). Their binding to phosphorylated activated GPCRs induces a conformational transition to an active state resulting in the release of their flexible C-terminal tail. Binding sites for clathrin and the adaptor protein (AP)-2 clathrin adaptor complex are then unmasked, which drive the recruitment of βarrs-GPCR complexes into clathrin-coated pits (CCPs). A conserved isoleucine-valine-phenylalanine (IVF) motif of the C-terminal tail controls βarr activation through intramolecular interactions. Here, we provide structural, biochemical and functional evidence in living cells that the IVF motif also controls binding to AP-2. While the F residue is directly involved in AP-2 binding, substitutions of I and V residues, markedly enhanced affinity for AP-2 resulting in active βarr mutants, which are constitutively targeted to CCPs in the absence of any GPCR activation. Conformational change and endocytic functions of βarrs thus appear to be coordinated via the complex molecular interactions established by the IVF motif.

Key words: AP-2, arrestin, clathrin, clathrin-coated pits, endocytosis, G-protein-coupled receptor, live cell imaging

Received 24 July 2006, revised and accepted for publication 2 April 2007

Arrestins are highly conserved proteins among multicellular organisms that play a central role in the regulation of the activity of G-protein-coupled receptors (GPCRs), the largest family of plasma membrane receptors. Visual arrestin specifically regulates rhodopsin signaling in retinal cells, whereas nonvisual arrestins 2 and 3, also known as β-arrestin1 (βarr1) and β-arrestin2 (βarr2), respectively, control GPCR signaling and trafficking in all other tissues. Beta-arrestins (βarrs) were first characterized for their ability to uncouple G proteins from activated GPCRs, but more recent studies have established that they are also directly involved in signal transduction pathways, acting as multifunctional adaptor molecules. Additionally, βarr are involved in the endocytosis of most GPCRs, mediating their recruitment into clathrin-coated pits (CCPs) and their subsequent internalization through the clathrin-dependent pathway (reviewed in 1).

The multiple functions of βarr are tightly regulated by complex conformational changes (reviewed in 2). Beta-arrestins are composed of two globular domains (N and C), and a flexible, extended, C-terminal tail, which is locked on the globular domains, at the resting state, via a conserved isoleucine–valine–phenylalanine motif (IVF, residues 386–388 of bovine βarr1, 387–389 of rat βarr2) interacting with a hydrophobic pocket of the N-terminal globular domain (3–6). This conformation represents the inactive 'closed' cytoplasmic form of βarr in unstimulated cells. After agonist activation, the cytoplasmic regions of agonist-bound GPCRs are phosphorylated by specific kinases. Beta-arrestin then bind to agonist-activated, phosphorylated GPCRs at the plasma membrane. Beta-arrestin binding to the phosphate groups disturbs intramolecular interactions and promotes a global conformational change of βarr leading to their active 'open' conformation. According to the most widely accepted model (2,7), the C-terminal tail of βarr is released in the active conformation (8,9), unmasking βarr-binding sites for clathrin and for the β2-adaptin subunit of the adaptor protein (AP)-2 clathrin adaptor complex (10,11), the latter playing a crucial role in the recruitment of GPCR/βarr complexes into CCPs (12).

The fact that the switch of βarr to the active open conformation is associated with the release of the C-terminal tail and its subsequent interaction with the endocytic machinery suggested that the two events might be regulated by common molecular motifs. Constitutively active mutants of both visual and nonvisual arrestins have been described, which display very low sensitivity for the phosphorylation status of GPCRs (13–15). Interestingly, these mutations targeted the conserved IVF motif, locking arrestins in their active open conformation and were immediately adjacent to amino acid residues shown to be involved in the interaction between the βarr and the β2-adaptin subunit of the AP-2 complex [F392/F391 and R396/R395 of rat βarr2 or bovine βarr1 (12,16)].

In the present study, we have used the already accessible structural data obtained for native βarr (5,6,17), including those we recently obtained for a βarr-derived peptide in complex with the ear domain of the β2-adaptin subunit of the AP-2 complex (18), to investigate the exact function of the residues of the IVF motif in both activation transition and AP-2 binding. The data obtained revealed an unexpected and complex function of the I and V residues within this motif, which appear to negatively control binding to AP-2. Mutagenesis of these residues resulted in constitutively activated forms of βarrs, which were used to investigate mechanistic models for βarr activation and CCP targeting.

Results

The IVF motif of βarrs directly participates and regulates binding to the β2-adaptin ear domain

In the solved structure of full-length bovine βarr1 (6,17), density for most of the residues of the C-terminus was lacking except for the region encompassing residues 383–399, which includes the IVF motif and the residues previously shown to be required for AP-2 binding (F391 and R395; Figure 1). This region was found in close interaction with both N- and C-terminal globular domains in its extended conformation (resting βarr). Some residues, such as F391 and R393, specifically contribute to this intramolecular interaction. The side chain of F391 projects into a hydrophobic pocket lined by several hydrophobic residues (F9, the aliphatic component of R25 and L166), while the side chain of R393 projects into a separate cavity and appears to establish links between the two globular domains (R25, D26, H295, D297). These observations are consistent with previous functional studies, which identified F391 and R393 as conformation-regulating residues (14,19,20). The IVF motif also contributes to the intramolecular interaction but with significant difference among the I, V and F residues. Indeed, the F is completely masked inside a pocket formed by hydrophobic residues of the N-terminus of the molecule (Y21, L104, L108), the I only interacts with the V8 residue of the N-terminus, while the V is completely accessible and does not establish any intramolecular contact (Figure 1C). The respective contribution of these residues in maintaining the closed conformation of βarr has not been fully investigated, although the concomitant mutation of all three residues into alanine resulted in a constitutively active form of βarrs (13–15).

The solved structure of an IVF-containing C-terminal βarr peptide (383–399) in complex with the ear domain of β2-adaptin (18 and see below) revealed a major conformational change compared with the resting state. Upon association with β2-adaptin, the peptide forms an α-helix,

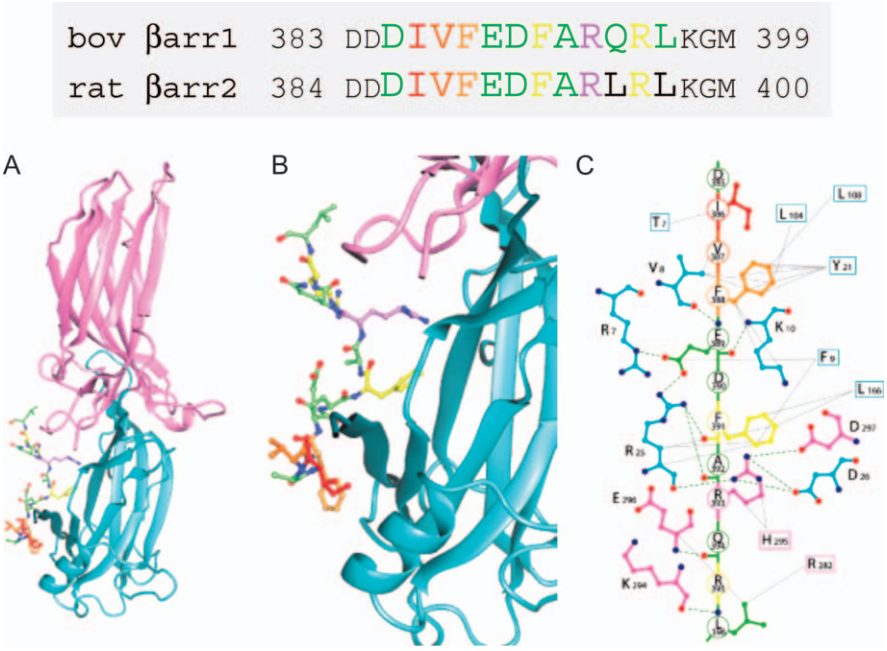

Figure 1: Structure of bovine βarr1 and intramolecular interactions of C-terminal tail residues. Top: Residues of the 383–399 region of bovine βarr1 and the 384–400 region of rat βarr2 are aligned [red to orange: the IVF motif, yellow: AP-2 binding, purple: R393 and bold black: NES (βarr2)]. A) 3D structure of bovine βarr1 adapted from Milano et al. (17). The N-terminal and C-terminal globular domains are in blue and pink, respectively, and residues of the C-terminal tail were colored as indicated above. B) Enlarged view focusing on the residues of the C-terminal tail, which interact with both N- and C-terminal globular domains. C) Map of the interactions involving the residues of the C-terminal tail. Potential hydrogen bonding (dashed green lines) and hydrophobic (gray lines) interactions are shown along a linear display of the DIVFEDFARQRL peptide.

in which the F residue of the IVF motif establishes direct contacts with a hydrophobic pocket of the β2-adaptin ear platform subdomain, a finding suggesting its direct involvement in AP-2 binding. As these observations indicate that the IVF motif participates in the regulation of both activation-dependent conformational change and endocytic functions of βarr, we investigated the role of each residue of the IVF motif in both AP-2 binding and activation state of βarr. The activation of the βarr molecule releases the AP-2-binding domain contained in the C-terminal tail from its intramolecular interactions (8,9). Therefore, mutations of any of the residues implicated in the control of this process in the context of the full-length molecule may affect AP-2 binding either directly or indirectly by affecting the accessibility of the AP-2-binding site. We therefore prepared constructs corresponding to the C-terminal tail of βarr, in which only direct effects on AP-2-binding capacities would specifically be tested. For theses studies, we principally used the βarr2 isoform as model instead of βarr1, which most studies have used previously. Indeed, βarr2, which is almost identical to βarr1 in terms of amino acid conservation within the IVF- and AP-2-binding-site-containing region, was reported to possess additional isoform-specific functions. These include constitutive nucleocytoplasmic shuttling capacity, which is controlled by a nuclear export signal (NES) adjacent to the IVF motif and the AP-2-binding site. The F392 residue (rat βarr2) is involved in both nuclear shuttling and AP-2 binding (16,21,22). The isoform-specific nuclear shuttling of βarr2 allows a more detailed structure–function analysis of the residues within this region (see below).

To simplify the description of the mutations generated in either βarr1 and/or βarr2, we used the following nomenclature: single alanine substitutions within the IVF motif are termed AVF, IAF and IVA, the AAF mutant corresponding to the double substitution of I and V and 3A representing the triple substitution. For the residues directly involved in the binding to β2-adaptin, residues of the concerned peptide were numbered as follow: D3xxF6xxF9xxxR13 (Figure 1).

The C-terminal tail of βarrs, which corresponds to an extended, partially structured flexible domain in the native molecule (5,6,17) (Figure 1A,B), contains both clathrin- and AP-2-binding sites (11,23). Previous reports showed that a fragment of βarr1, corresponding to the C-terminal tail (residues 319–418), displayed a punctate distribution co-localizing with clathrin (24), suggesting its constitutive targeting to CCPs. These data therefore support the hypothesis that the C-terminal tail of βarrs contains a sufficient CCP targeting signal. This hypothesis was directly confirmed by the fact that a green fluorescent protein (GFP)-tagged constructs of the C-terminal tail of rat βarr1 and βarr2 (residues 315–418 and 317–410, respectively) were found to colocalize with specific markers of plasma-membrane-associated CCPs, such as the AP-2 complex (Figure 2A,B and Figure S1A,B), showing that the C-terminal tail of both βarrs indeed contains a sufficient signal for CCP targeting. The functional motif required for CCP targeting activity was mapped using a series of GFP-tagged C-terminal tail deletions [previously described in (21)]. The CCP targeting activity of the C-terminal tail was completely lost when residues 391–400 were deleted, as shown by the diffuse staining of the resulting construct (Figure S1C,D). This 10 amino acid stretch has previously been identified as an AP-2-binding region (12,16), therefore, indicating that binding to the AP-2 complex is required for the CCP targeting activity of the C-terminal tail. In addition, these data suggest that the upstream clathrin-binding site [LIEFD motif, residues 374–378 (23)] is not sufficient on its own for this function. The requirement of both AP-2 and clathrin binding for CCP targeting was further analyzed by introducing in the C1 fragment point mutations, which target either to the residues known to be required for binding to the β2-adaptin ear domain (F9 and R13) or to the clathrin N-terminal domain (LIEF) (12,16,23). Both mutations similarly affected the localization of the resulting constructs, which showed diffuse cytoplasmic distributions, and loss of colocalization with AP-2 (Figure 2 C–F and data not shown). Taken together, these results show that AP-2 and clathrin-binding sites are both required but not sufficient individually for CCP targeting and likely co-operate for this function.

Because AP-2 binding is required for efficient targeting of the C-terminal tail constructs to CCPs, point mutations of the IVF motif were introduced in the context of the GFP-tagged C-terminal tail construct of βarr2 and the steady-state localization of the corresponding chimeras was analyzed by immunofluorescence. Mutation of the I (AVF) and V (IAF) residues of the IVF motif did not affect the CCP targeting of the βarr2 C-terminal tail, as shown by their plasma membrane punctate distribution, colocalizing with endogenous AP-2 complexes (Figure 2 G–J). In contrast, the IVA mutation resulted in complete loss of the punctate plasma-membrane-associated distribution (Figure 2K,L). These results demonstrate that the F residue of the IVF motif is necessary for the CCP targeting activity of the βarr2 C-terminal tail, whereas I and V residues do not seem to play a direct role in this process.

The individual impact of each of the residues of the IVF motif in AP-2 binding was also directly tested *in vitro*. The same point mutations of the IVF motif were introduced in glutathione S-transferase (GST) fusions containing the C-terminal tail of βarr2, and the resulting chimeras were used to precipitate AP-2 complexes from cell lysates. As expected, mutation of the F residue either in the IVA or in the 3A βarr2 mutants reduced the capacity of the C-terminal tail to interact with AP-2 complexes (Figure 3A, compare lane 1 with lanes 3 and 4), confirming that the F residue is required for optimal AP-2 binding (18,25). Surprisingly, mutation of the I residue (AVF) resulted in increased AP-2 binding efficiency compared

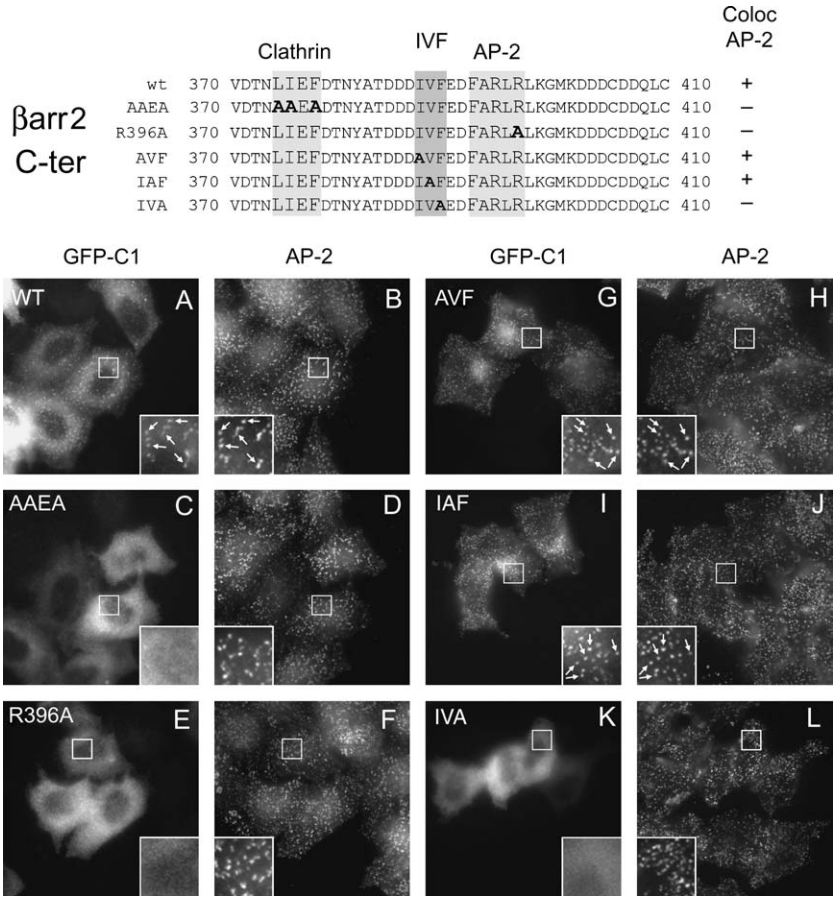

Figure 2: Role of the IVF motif in CCP targeting. Upper panel: Sequences of C-terminal fragment of rat βarr2 and of mutants of the IVF motif, the AP-2 or clathrin-binding site mutants. Lower panel: Hela cells were transiently transfected with GFP-tagged C1 (A and B) or mutated C1, with substitutions in the clathrin-binding site 'AAEA' (C and D), the AP-2-binding site 'R396A' (E and F), or in the IVF motif 'AVF' (G and H), 'IAF' (I and J) and 'IVA' mutants (K and L). Cells were fixed and directly processed for fluorescence microscopy with anti-AP-2 antibody as in Figure S1. Insets show higher magnifications of representative areas. Colocalized spots are indicated by arrows. In A, C, E, G, I and K, green fluorescence emitted by GFP (βarr2). In B, D, F, H, J and L, red fluorescence emitted by Alexa594 (AP-2).

with wild type (Figure 3A, compare lanes 2 and 1). A similar phenotype was also observed for both IAF and AAF mutants (Figure 3A, lanes 8 and 9), suggesting that the I and the V residues of the IVF motif might negatively regulate AP-2 binding.

The effect of the mutations of the IVF motif on AP-2 binding were more precisely quantified by isothermal titration calorimetry (ITC), a technique, which allows the calculation of the equilibrium association or dissociation constants for interactions (26,27). Confirming the findings obtained with GST pull downs, the AVF, IAF and AAF mutant peptides showed fivefold increased affinity for AP-2 compared with the wild-type peptide (0.5 μM and 2.5 μM, respectively, Figure 3B and data not shown). In contrast, in the same conditions, mutation of the F residue (IVA) resulted in a complete loss of binding of the resulting peptide to the isolated β2-adaptin ear domain (Figure 3B).

Altogether, these results show that, independent of its role in conformational regulation, the IVF motif tightly regulates AP-2 binding with the I and the V residues negatively regulating β2-ear-binding domain while F being directly involved in this interaction.

I/V mutants of the IVF motif localize in CCPs at steady state

The residues of the IVF motif were initially described for their role in the docking of the C-terminal tail onto the globular domains and, therefore, in the regulation of the activation state of βarrs (see above). To directly test the role of each residue of the IVF motif, in the context of the entire molecule, the distribution of full-length βarr2 mutants of the IVF motif was studied at steady state. These mutants included a construct in which all three residues of the IVF motif were mutated to alanine (3A), and which was previously characterized as a constitutively active mutant capable of binding *in vitro* to agonist-activated nonphosphorylated receptors (13,19). We reasoned that if the C-terminal tail contains a sufficient CCP targeting signal (see above), then mutants of βarr with a released C-terminal tail should be targeted to CCPs in the absence of agonist stimulation, except if the mutated residues are also involved in AP-2 binding.

As shown in Figure 4 and in a previous report (21,28), in the absence of specific agonist stimulation, wild-type βarr2 is diffusely distributed in the cytoplasm (Figure 4A). Alanine substitution of either the I (AVF) or the V (IAF) residues or both (AAF) of the IVF motif resulted in

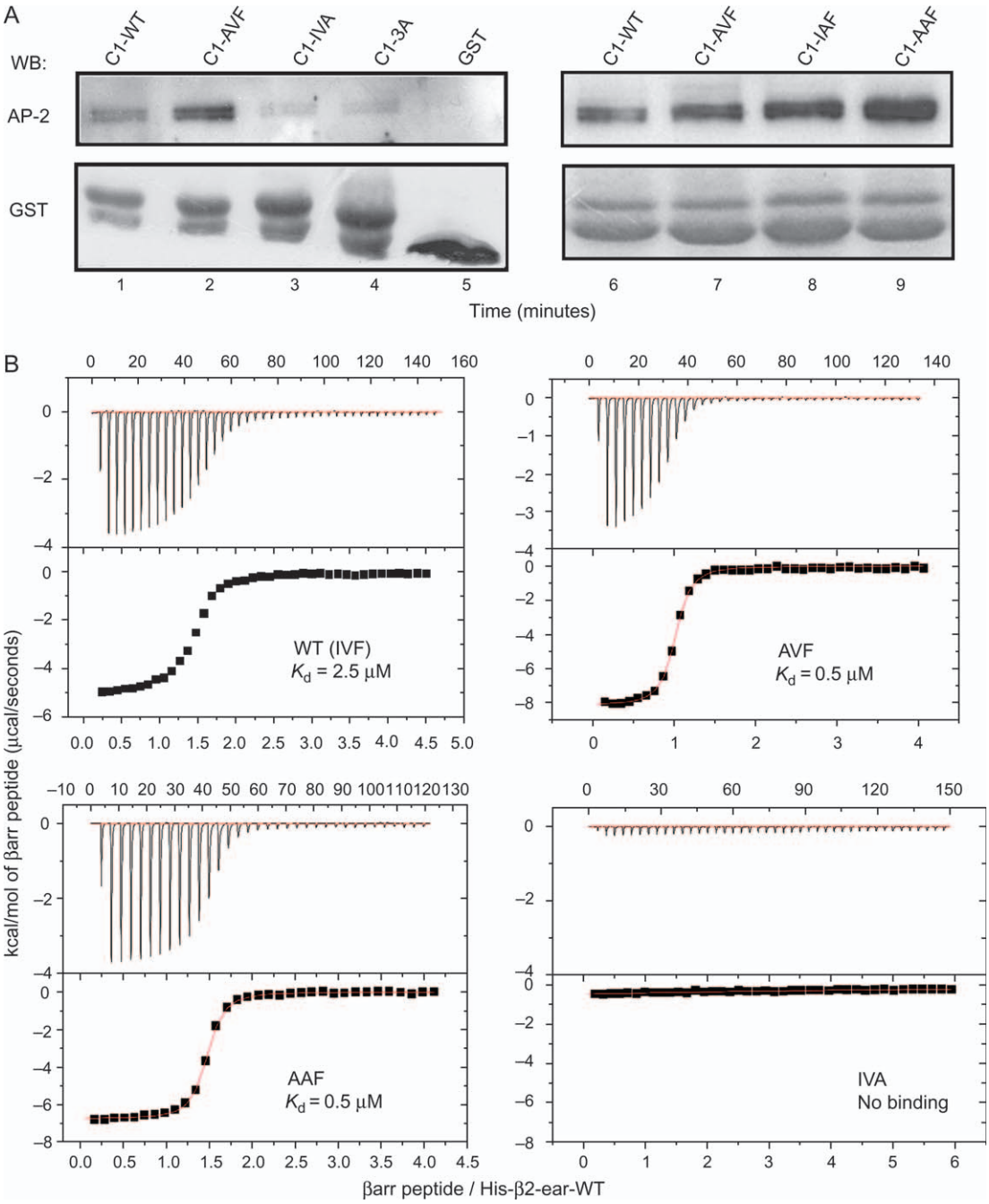

Figure 3: Role of the IVF motif in AP-2 binding. A) GST fusion proteins corresponding to either wild type (lanes 1 and 6) or AVF (lanes 2 and 7), IVA (lane 3), 3A (lane 4), IAF (lane 8) and AAF (lane 9) mutants of the βarr2 C-terminal tail, or GST (lane 5) alone, were used to precipitate AP-2 from HeLa cells lysates. Upper panel: Bound proteins were separated via SDS-PAGE and the presence of bound AP-2 complexes was assessed by Western blotting using an anti-αα-adaptin antibody. Lower panel: Before incubations with antibodies, the nitrocellulose membrane was first stained with ponceau red for quantification of GST fusion proteins. B) Affinities of βarr peptides (wild type, AVF, AAF and IVA as indicated) for wild-type β2-adaptin ear domain were measured by ITC.

a punctate distribution of βarr mutants at the plasma membrane (compare C, D and F to A), suggesting their constitutive localization in CCPs. This hypothesis was confirmed by colocalization studies by epifluorescence microscopy. As expected, both AVF, IAF and AAF mutants were colocalized with endogenous AP-2 in spots at the plasma membrane (Figure S2 and Figure 4H,K). In contrast, mutants of the F residue of the IVF motif including both 3A and IVA showed similar steady-state diffuse cytoplasmic distribution as wild-type protein and the

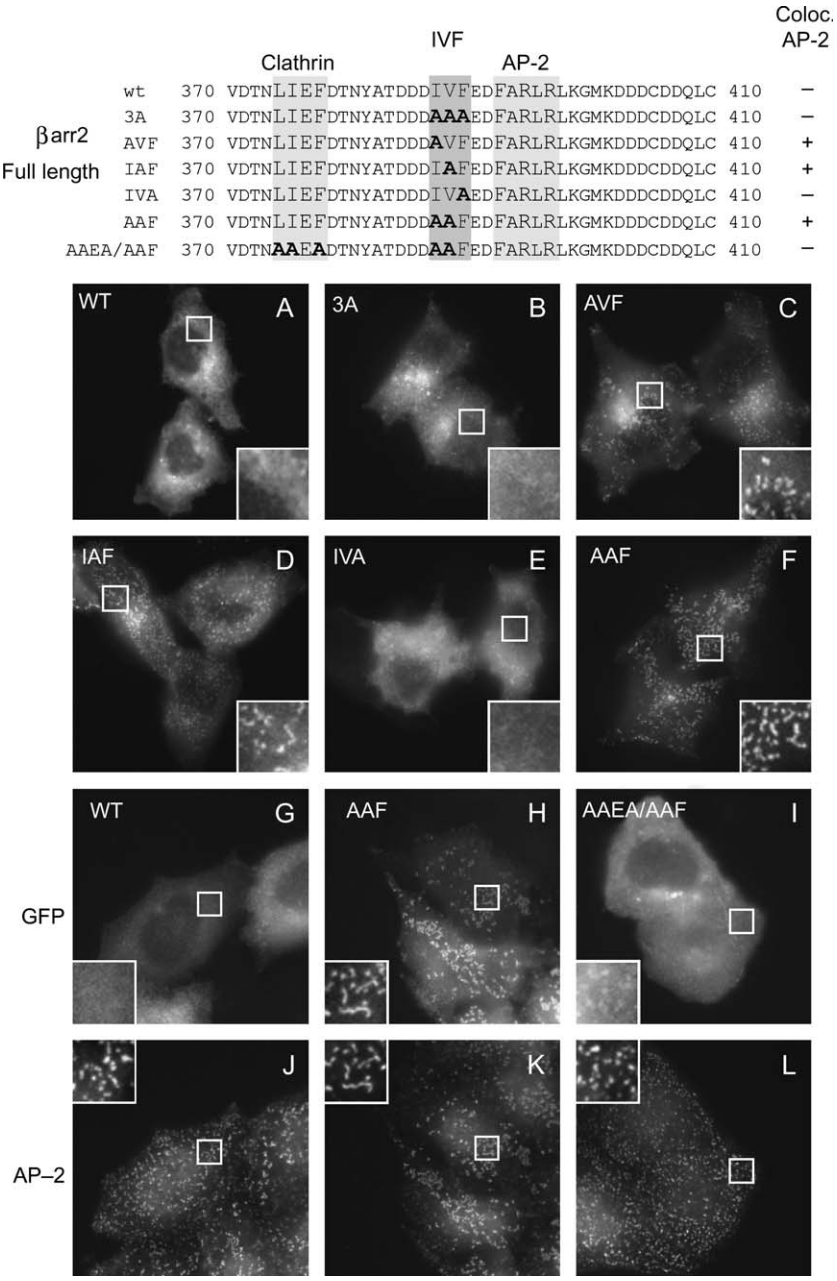

Figure 4: Plasma membrane distribution of IVF motif mutants. Upper panel: Sequences of wild type rat βarr2 and of mutants of the IVF motif. Lower panel: Hela cells were transiently transfected with wild type (A, G and J), 3A (B), AVF (C), IAF (D), IVA (E), AAF (F, H and K) and AAEA/AAF (I and L) GFP-tagged βarr2 constructs. Cells were fixed and directly processed for fluorescence microscopy or stained with an anti-AP-2 antibody as in Figure 1. In A, B, C, D, E, F, G, H and I, green fluorescence emitted by GFP (βarr2). In J, K, and L, red fluorescence emitted by Alexa594 (AP-2). Insets show higher magnifications of representative areas of the adherent surface of the cells.

absence of colocalization with AP-2 (Figure 4B,E and Figure S2). Together with the results showing that the F residue of the IVF motif is required for efficient AP-2 binding, and others showing that mutation of the R396 residue abolished constitutive colocalization with AP-2 of I/V mutants (data not shown), these results indicate that AP-2 binding is required for the constitutive CCP targeting of I/V mutants.

In agreement with the results obtained with the C-terminal tail constructs (Figure 2), clathrin binding is also necessary for constitutive CCP targeting of the AAF mutant. Indeed, the additional mutation of the clathrin-binding site, reverted the AAF phenotype, resulting in a diffuse cytoplasmic distribution (AAEA/AAF, Figure 4I,L) similar to wild-type βarr2 (Figure 4A,G). Quantification of the colocalization by measurement of GFP fluorescence inside AP-2-positive spots (see *Materials and Methods*) confirmed these observations (Figure 7M). While the AAF mutant was accumulated in CCPs (normalized fluorescence of 1.33), mutation of the clathrin-binding site (AAEA/AAF) resulted in a drop of normalized fluorescence to 1.08 ($p = 3.10^{-68}$), a value similar to wild-type βarr2 in the absence of stimulation (1.03) and therefore to background fluorescence.

As AVF, IAF and AAF mutants showed similar patterns of subcellular localization and AP-2 binding (Figures 3 and 4), subsequent analyses were principally conducted on the

AAF mutant. The constitutive CCP localization of the AAF mutant was further confirmed using total internal reflection fluorescence microscopy (TIR-FM). This technique restricts the excitation of the samples to a 100-nm region immediately adjacent to the coverslip on which the cells are adhering. Thus, only a region of the cell, which includes the plasma membrane and a fraction of the underlying cytoplasm, is illuminated (reviewed in 29). TIR-FM is therefore a powerful tool to follow plasma-membrane-associated endocytic events (reviewed in 30,31). HeLa cells were cotransfected with both the GFP-tagged βarr2 AAF mutant and a DsRed-tagged clathrin construct, fixed, stained for endogenous AP-2 complexes and observed by TIR-FM. The AAF mutant was found in small spots dispersed on the plasma membrane (Figure 5A), which colocalized with both clathrin–DsRed and endogenous AP-2 complexes (Figure 5 B,C). Colocalization was quantified by measuring the fluorescence intensity of both clathrin–DsRed and AP-2 inside GFP-positive AAF spots. The spots corresponding to the AAF mutant contained proportional amounts of both clathrin and AP-2 (Figure 5E), confirming the localization of the AAF mutant in CCPs. The specificity of the CCP localization was further demonstrated by the fact that in the same conditions, the AAF mutant did not colocalize with marker of caveolae (mRFP-caveolin1, Figure S3).

The AAF mutant of βarr2 is in an active open conformation

Taken together, the results described above show that mutation of the I, the V or IV residues of the IVF motif resulted in constitutive localization of βarr in CCPs in the absence of any receptor stimulation. This constitutive CCP localization is in agreement with the proposed role of these residues in the control of the activation state of βarr, their mutation into alanine resulting in a constitutive partially active phenotype, allowing binding to nonphosphorylated activated receptors (14,19). The mutation of the I/V residues is expected to result in a constitutive active open molecule with its C-terminal tail released and accessible to the AP-2 complex. In contrast, the additional mutation of the F residue (mutant 3A) would likely result in a similar active open mutant unable to bind to AP-2 and therefore not targeted to CCPs (see above). This hypothesis was first verified *in vitro* by testing the AP-2-binding properties of GST fusions encoding wild-type βarr2 or mutants of the IVF motif in the full-length context. As expected, I/V mutants showed increased binding to AP-2 compared with wild-type protein. This binding was specific because it was displaced by the addition of purified β2-adaptin ear domain (Figure 6A). As expected, mutation of the F residue (IVA and 3A) resulted in a drastic reduction of AP-2 binding (Figure 6A). Together, these results support the hypothesis that the I/V mutants are constrained in the open conformation, whereas 3A, although being in the open conformation, is unable to bind to AP-2. Alternatively, the increased binding to AP-2 of the I/V mutant could result from intrinsic increased affinity for AP-2, as indicated by experiments conducted with GST fusions of the isolated C-terminal tail or βarr-derived peptides (Figure 3).

The accessibility of the C-terminal tail of the AAF βarr2 mutant to β2-adaptin binding was directly investigated using another approach. We reasoned that if the C-terminal tail of βarr2 is indeed released in the I/V mutants, it would bind to an isolated ear domain of β2-adaptin. Residues involved in binding to β2-adaptin and nuclear export lay in the same region of the C-terminal tail of βarr2. Because the F residue at position 392 of βarr2 (position F9 of the C-terminal peptide) is involved in both functions (16,22), binding of the βarr2 C-terminal tail to the β2 ear domain of AP-2 should mask the NES. This masking should inhibit the constitutive nuclear export of βarr2 and therefore cause its accumulation in the nucleus because of its active nuclear import (21). The AAF βarr2 mutant was excluded from the nucleus at steady state (Figure 6F, arrowhead, and Figure S4B) and treatment of AAF βarr2 expressing cells with leptomycin B, a drug which blocks nuclear export (32), resulted in its accumulation in the nucleus as for wild-type βarr2 (Figure S4). Similar results were also observed for both AVF and IAF (data not shown) mutants, showing that mutation of I or V residues of the IVF motif, and therefore activation of βarr2, did not interfere with its constitutive nucleocytoplasmic shuttling. Coexpression of the AAF mutant with the β2-adaptin ear domain resulted in a clear nuclear accumulation of the βarr2 mutant (Figure 6E–G, arrows), similar to that observed upon treatment with leptomycin B (Figure S4). This nuclear accumulation was observed in almost every cell, in which the AAF mutant was coexpressed with the β2-adaptin ear domain but not in cells expressing the AAF mutant alone (Figure 6E–G, arrowhead). As expected, wild-type βarr2 was not translocated in the nuclei of cells expressing the β2-adaptin ear domain (Figure 6B–D). Combined, these results confirm that the C-terminal tail of βarr2 is much more accessible to the β2-adaptin ear in the AAF mutant. Accordingly, mutation of the I and V residues of the IVF motif indeed results in a constitutively active open form of βarr2. Finally, confirming the specificity of the observation and in agreement with the competition observed *in vitro* (Figure 6A), the constitutive CCP targeting of the AAF βarr2 mutant was lost in cells, which expressed high levels of β2-adaptin ear domain (Figure 6H–J, arrows). It is interesting to note that in the same field, cells expressing moderate levels of β2-adaptin ear domain showed clear translocation of the AAF mutant in the nucleus while CCP targeting was not affected (Figure 6H–J, arrowheads).

Active mutants, CCP recruitment and internalization of GPCR

The results presented above provided a new tool to test hypothetical models of βarr functioning. Indeed, in the current models, βarr binding to agonist-activated phosphorylated receptors is supposed to result in the activation

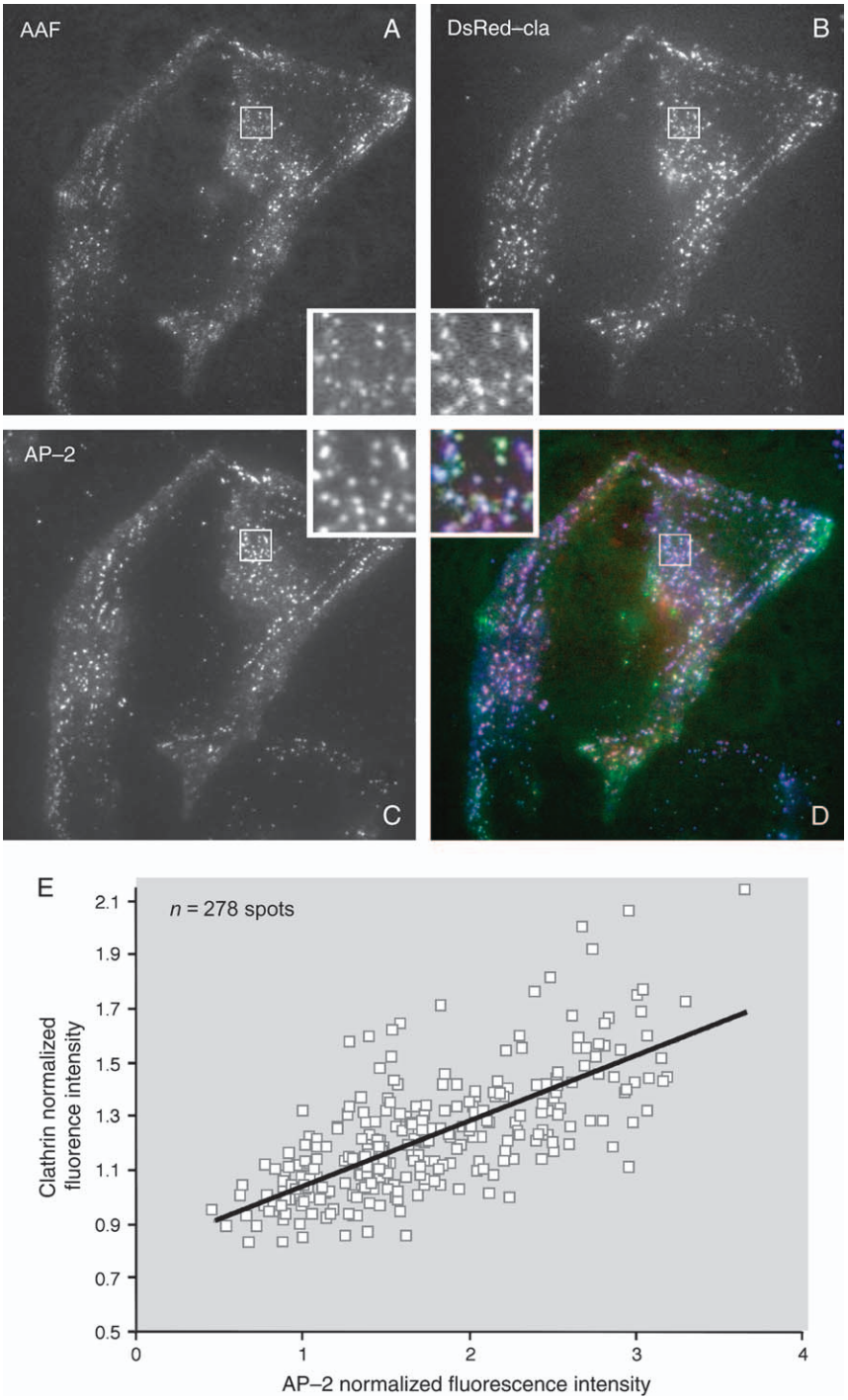

Figure 5: The AAF mutant localizes in CCPs at steady state. HeLa cells were transiently transfected with both A) the GFP-tagged βarr2 AAF mutant construct and B) the DsRed-tagged clathrin light chain construct. C) After fixation and permeabilization, the cells were stained for endogenous AP-2, revealed by an Alexa633-labeled goat anti-rabbit secondary antibody. Cells were imaged by total internal reflection fluorescence microscopy. Insets show higher magnification of a representative area. D) In the overlay image, the fluorescence corresponding to GFP is in green (AAF mutant), DsRed in red (clathrin) and Alexa633 in blue (AP-2). E) Normalized fluorescence intensities were calculated for both AP-2 and clathrin in 278 AAF spots.

of the molecule with release of its C-terminal tail (1,2). The accessibility of AP-2 and clathrin-binding sites would allow the recruitment of βarr/GPCR complexes into preformed CCPs (28,33). The AAF mutant bypasses the agonist activation step, already being in the active conformation and accumulated in CCPs. We asked whether this activation mutant would also be able to drive GPCR recruitment into CCPs without agonist activation. Cells were cotransfected with plasmids encoding GFP-tagged wild type or βarr2 mutants together with a thyrotropin-releasing hormone receptor (TRH-R) construct carrying an extracellular N-terminal vesicular stomatitis virus (VSV) tag, which we previously used to follow recruitment of βarr/GPCR complexes in CCPs (28). Activated TRH-R undergoes clathrin-mediated internalization and remains stably associated with βarrs, which are therefore recruited on endosomes

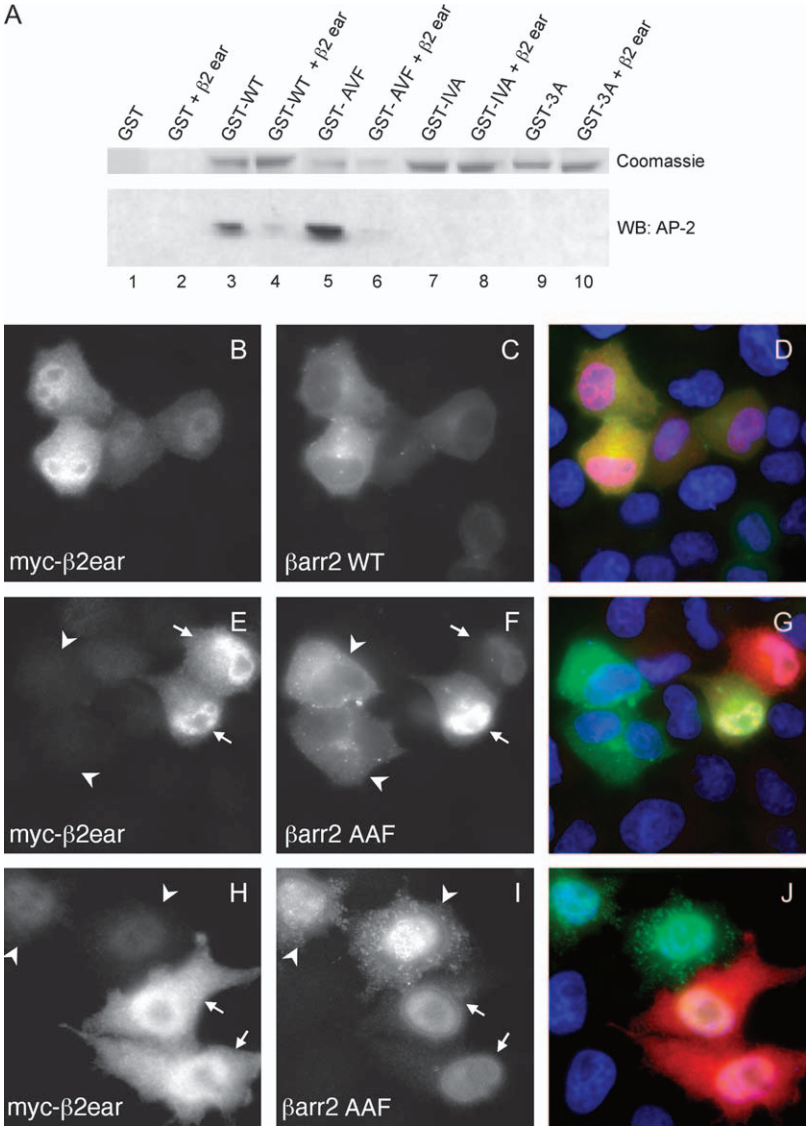

Figure 6: The AAF mutant is in the active open conformation *in vivo*. A) GST (lanes 1 and 2) or GST fusion proteins corresponding to either wild type (lanes 3 and 4) or AVF (lanes 5 and 6), IVA (lanes 7 and 8) or 3A (lanes 9 and 10) mutants, were used to pull-down AP-2 from HeLa cells lysates in the presence or not of an excess of histidine-tagged β2-adaptin ear domain. Upper panel: Bound proteins were separated on SDS-PAGE and the presence of bound AP-2 complexes was assessed by Western blotting using an anti-β-adaptin antibody. HeLa cells were transiently transfected with plasmids coding either for the GFP-tagged wild-type βarr2 (B–D) or for the AAF mutant (E–G) together with a myc-tagged β2-adaptin ear domain construct. After fixation, cells were stained with an anti-myc antibody revealed by Alexa594-labeled secondary antibody. In B, E and H, red fluorescence emitted by Alexa594 (myc-β2 ear). In C, F and I, green fluorescence emitted by GFP (βarr). In D, G and J, combined images. In B–G, the focus was made on the mid region of the cells to allow better observation of the nuclei. In H–J, the focus was made on the adherent surface of the cells to observe CCPs. In the two upper cells, which express low levels of β2-adaptin ear (arrows), AAF mutant is present in the nucleus and in CCPs. In the two lower cells (arrowheads), which express very high levels of β2 ear, AAF mutant was mainly nuclear and absent from CCPs.

after long-term TRH stimulation [type B receptor; (34,35)]. In cells expressing wild-type βarr2, in the absence of TRH, the TRH-R showed a diffuse distribution at the plasma membrane (Figure S5A, B) as previously described (28). A similar diffuse distribution of the TRH-R was observed in cells expressing the AAF mutant even if the arrestin mutant was effectively present in CCPs (Figure S5C,D). These results clearly indicate that expression of active mutants of βarr is not sufficient by itself to recruit unstimulated GPCRs in CCPs.

The effect of GPCR stimulation on the recruitment of arrestin constructs as well as the effect of the expression of the arrestin constructs on the recruitment of activated GPCR in CCPs were next investigated. Cells coexpressing TRH-R and GFP-tagged arrestin fusions were stimulated with TRH for 1 minute and stained for both TRH-R and AP-2 complexes. The distribution of the three markers in the same cells was analyzed by fluorescence microscopy and the relative accumulation of GFP-tagged βarr2 constructs inside CCPs was quantified by measuring the normalized GFP-associated fluorescence inside AP-2-positive spots (see *Materials and Methods*).

After TRH-R activation for 1 minute, wild-type βarr2 was, as expected, recruited into CCPs (>90% of total CCPs, data not shown) as shown by its extensive colocalization with AP-2 staining (Figure 7A,B) and increased normalized fluorescence intensity inside AP-2 spots, compared with resting conditions (Figure 7M; $p = 9.10^{-59}$). Clathrin-coated pit recruitment was dependent on both clathrin and AP-2 binding, as the AAEA/R396A double mutant showed a diffuse membrane staining upon TRH stimulation (Figure 7J,K) with fluorescence signal in AP-2 spots similar to background (Figure 7M). The distribution of the AAF mutant was not affected by TRH stimulation because

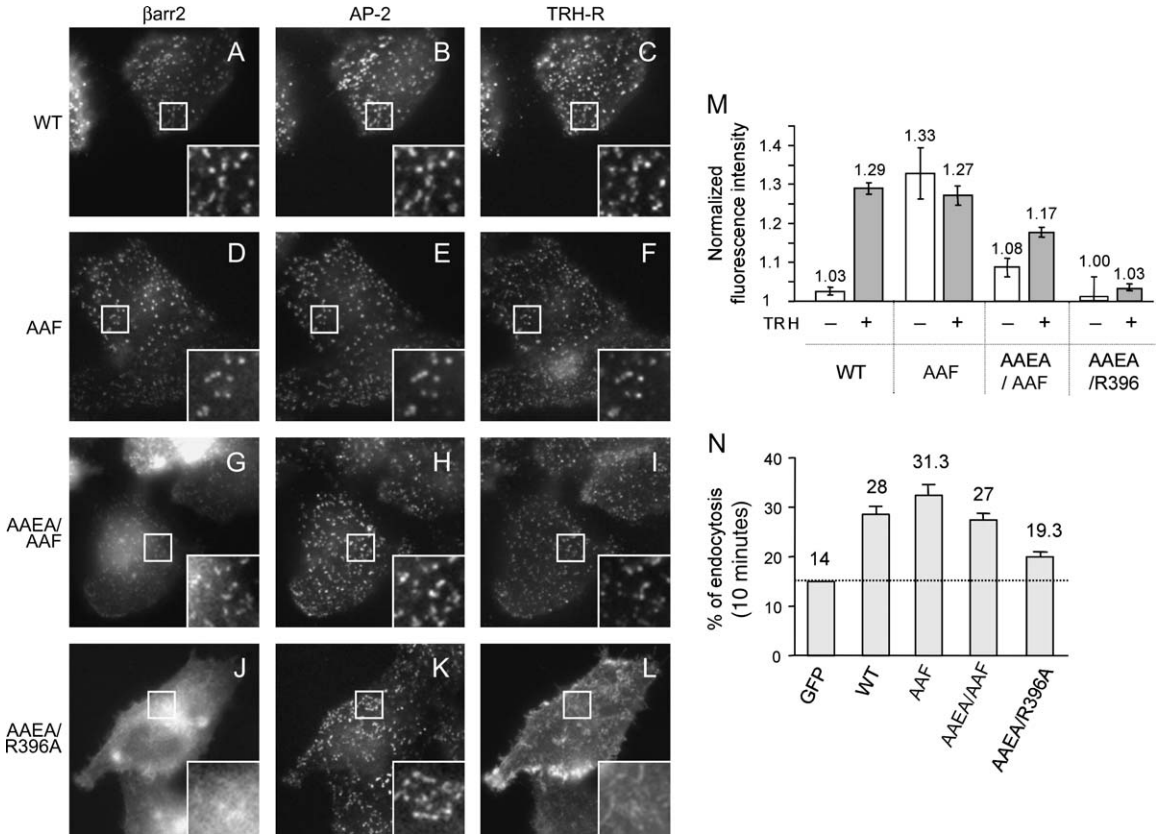

Figure 7: The AAF mutant recruits TRH-R in CCPs and mediates its agonist-promoted internalization. HeLa cells were transiently cotransfected with plasmids coding for a N-terminal VSV-tagged TRH-R and GFP-tagged wild-type βarr2 (A–C), AAF (D–F), AAEA/AAF (G–I) or AAEA/R396A (J–L). After 1-h incubation with a Cy3-labeled anti-VSV antibody at 4 °C, cells were shifted at 37 °C for 1 minute with 10 μM TRH, then washed in cold medium, fixed at 4 °C and stained with an anti-α-adaptin antibody, revealed by an Cy5-labeled donkey anti-mouse secondary antibody. In A, D, G and J, green fluorescence emitted by GFP (βarr2 constructs). In B, E, H and K, far red fluorescence emitted by Cy5 (AP-2). In C, F, I and L, red fluorescence emitted by Cy3 (TRH-R). The focus was made on the adherent surface of the cells to observe CCPs. Insets show higher magnification of representative areas. M) Fluorescence intensity of GFP inside AP-2 spots ($n = 300$, from at least three different cells) was measured and normalized with fluorescence intensity of GFP outside AP-2 spots as indicated in the Methods. Errors bars were obtained by calculating the standard error and relevance of the difference assessed with a Student *t*-test. N) Internalization of radioactive TRH was measured, as described in Materials and Methods, in cells coexpressing the VSV-tagged TRH-R and either GFP or GFP-tagged βarr2 fusions including wild type or AAF, AAEA/AAF or AAEA/R396A mutants. Cells were incubated with radioactive TRH at 4 °C, then washed in cold medium and then incubated for 10 minutes at 37 °C to allow internalization. Results are expressed as the percentage of initial total specific binding.

this construct was present in more than 90% of total CCPs (data not shown) and colocalized with AP-2 in both resting (Figure 4) and TRH-stimulated cells (Figure 7D,E). This observation was directly confirmed by the fact that normalized fluorescence intensity of the AAF mutant inside AP-2 spots remained similar in both conditions (Figure 7M, $p = 0.013$). Interestingly, the normalized fluorescence intensity inside AP-2 spots of wild-type βarr2 after agonist stimulation reached the same level as the AAF mutant in resting or stimulated cells ($p = 0.012$ and $p = 0.50$, respectively). This latter result shows that constitutive CCP targeting of the AAF mutant may represent the maximal possible recruitment of wild-type protein upon agonist stimulation of a receptor. In addition, while additional mutagenesis of clathrin-binding site significantly affected constitutive CCP targeting of the AAF mutant (Figure 7M, $p = 2.10^{-68}$), it only partially affected its recruitment into CCPs upon agonist stimulation, the normalized fluorescence inside CCPs being, in this case, significantly higher than for background but lower than for AAF (Figure 7M; $p = 0.0003$).

Using this microscopy-based approach, all the different βarr2 mutants except the AAEA/R396A double clathrin and the AP-2 mutant showed similar capacities to recruit activated TRH-R into CCPs as shown by colocalization of TRH-R with both AP-2 and βarr2 constructs upon agonist stimulation (Figure 7C,F,I,L). To directly compare the efficiency of each βarr2 construct to mediate the incorporation of activated GPCR in forming CCPs and clathrin-coated vesicles (CCVs), these constructs were tested in a TRH endocytosis assay (21). In this

assay, internalization of TRH from the plasma membrane was stimulated by expression of wild-type βarr2 (Figure 7N, compare GFP with wild type). The AAEA/R396A double mutant, which was not able to recruit TRH-R in CCPs after short TRH stimulation, was much less efficient than wild-type protein to stimulate TRH internalization (Figure 7N). In the same conditions, both constructs bearing the AAF mutation enhanced TRH internalization to a level comparable to that promoted by wild-type βarr2 (Figure 7K), suggesting that the AAF mutant showed similar capacity than wild-type βarr2 for GPCR endocytosis.

The above results confirm that the AAF mutant is fully functional in terms of GPCR endocytosis, being able to recruit activated GPCRs to CCPs and to drive their internalization into endosomes (see Figure S5E–H). These results also highlight that, as predicted by the current models, agonist activation is necessary to allow the recruitment of GPCRs into CCPs.

Dynamic analysis of the AAF mutant

As the AAF mutant is constitutively targeted to CCPs, to a level similar to that observed for wild-type βarr2 upon receptor stimulation, we analyzed and compared its dynamic distribution at the plasma membrane, relative to that of clathrin. Indeed, recent studies have evaluated the dynamics of CCPs and CCVs using fluorescent-tagged clathrin or AP-2 constructs by both fluorescence recovery after photobleaching (FRAP) and live cell TIR-FM imaging (reviewed in 30,31).

The half-life of the AAF mutant in CCPs was analyzed by FRAP in living HeLa cells. Small regions of the adherent surface of the cells expressing GFP-tagged AAF mutant were photobleached (Figure 8A, and data not shown) and the recovery of fluorescence was measured as described in Methods. The recovery of AAF mutant was rapid (halftime of ∼17.6 seconds) and efficient (85.3%; Figure 8B). These values are very similar to those previously measured for clathrin (16.2 seconds, 80%) or AP-2 (14.4 seconds, 81%; 36,37). These results confirm that despite their apparent lack of movement (Figure 8A,D), the CCPs at the adherent surface undergo rapid turnover and that the AAF mutant follows a turnover similar to that of AP-2 and clathrin. We next used live cell TIR-FM imaging to follow the AAF mutant in real time relative to that of clathrin. In this system, CCPs appear as static clathrin spots (CS), whereas forming CCV are represented by CS, which rapidly disappear (few seconds), as a result of their movement deeper into the cytoplasm out of the evanescent field (reviewed in 30,31). In live HeLa cells, the GFP-tagged AAF mutant colocalized with DsRed-tagged clathrin (Figure 8C) as described above in fixed cells (Figure 5). However, the AAF βarr2 mutant was absent from some CS (Figure 8D, for an example). Dynamic analysis revealed that clathrin-positive and AAF-negative spots corresponded to CS disappearing from the evanescent field during the observation (Figure 8C). In these spots, clathrin-associated fluorescence rapidly decreased, while fluorescence remained close to background before, during and after disappearance of the dynamic CS (Figure 8E). The presence of the AAF mutant in the different populations of CS was further analyzed by measuring the mean normalized fluorescence intensity corresponding to the βarr2 mutant within each type of CS population. As shown in Figure 8F, the mean normalized fluorescence intensity of AAF mutant dropped from 1.55 in static CS to 1.15 in disappearing CS, the latter value being close to background fluorescence. These results show that while the constitutively active AAF βarr mutant is clearly enriched in static CS in the absence of agonist activation, it is not incorporated into disappearing CS.

The latter observation strikingly paralleled those we previously made following AP-2 complex by TIR-FM showing that the AP-2 was enriched in static CS and nearly absent in those which are disappearing (38,39). These observations led to a new model for CCP/CCV formation in which AP-2 complexes are accumulated in CCPs but not incorporated in forming CCV (30). The fact that the activated mutant of βarr behaved exactly as AP-2 is not surprising because its localization in CCPs directly depends on their interaction. It also suggests that βarr would be preliminary targeted to CCPs and that incorporation into forming CCV (disappearing CS) would require further receptor stimulation, again stressing the central role of the receptor and/or receptor activation in the endocytic trafficking of βarr.

Discussion

The results presented in this study reveal that the highly conserved IVF motif found in the flexible C-terminal tail of all arrestin family members, function as a molecular switch, which couples the activation of βarrs and their capacity of interacting with components of the endocytic machinery.

The recently solved structure of the β2-adaptin ear domain, complexed to a peptide corresponding to the IVF-containing region, revealed that the peptide undergoes a major conformational change upon AP-2 binding, consisting of a transition from the extended conformation in the native molecule to an α-helix (18). In addition, Edeling et al. recently showed that autosomal recessive hypercholesterolemia protein (ARH), an adaptor for the low-density lipoprotein receptor, binds β2-adaptin ear domain through a peptide that also adopts an α-helix conformation (25). However, the structure of native ARH is unknown, precluding any conclusion on the possible conformational change of ARH upon AP-2 binding. The α-helix transition of βarr upon AP-2 binding involves the residues D3 to L14, and thus includes all the residues directly involved in the

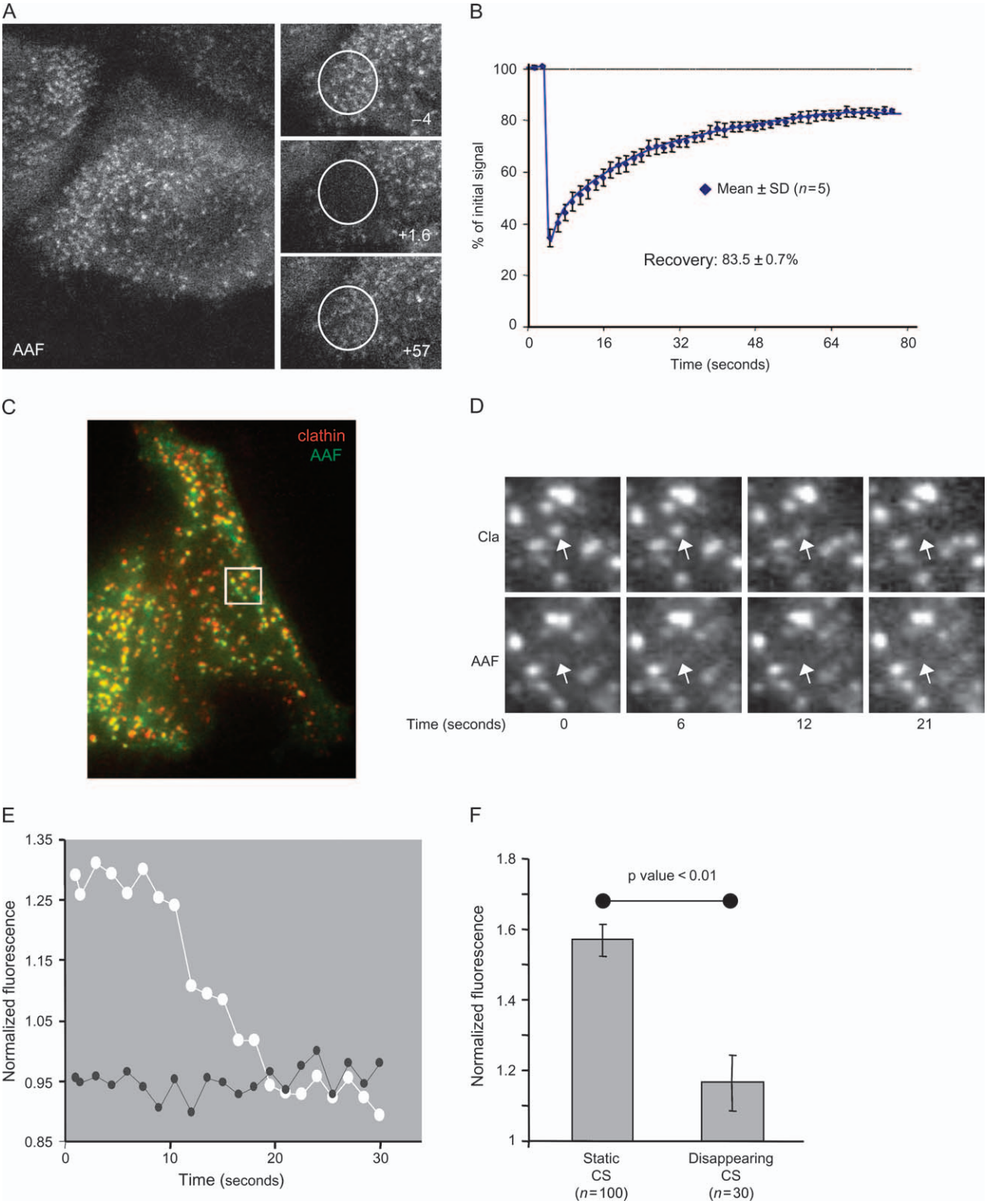

Figure 8: Legend on next page.

interaction with the β2-adaptin ear domain, namely F6 (the third residue of the IVF motif), F9 and R13 (Figure 9). Interestingly, this region corresponds to the only part of the flexible C-terminus of βarr1 (D1-G16), to be structured in the crystal of the native molecule, likely because of intramolecular interactions (see *Introduction*). Thus, the

conformation of this region appears to depend upon the binding partner with which βarr is complexed. Following agonist activation and binding to agonist-activated GPCRs, βarr undergoes two major conformational changes, including the release of the C-terminal tail region from its interaction with the N- and the C-terminal globular domains (8,9) and an α-helix transition of the AP-2-binding region upon interaction with the ear domain of β2-adaptin (18). It is therefore likely that binding to β2-adaptin ear stabilizes the active conformation of βarrs by impeding the folding back of the C-terminal tail and therefore return of the molecule to the inactive state. This hypothesis is supported by the fact that βarr residues directly involved in the interaction with the β2-adaptin ear also point inside the βarr molecule (F9) or are in close contact with the globular domains of the native molecule at the resting state (F6 and R13, compare Figures 1 and 9). Because the same residues cannot be involved in two distinct interactions simultaneously, binding of βarrs to β2-adaptin ear likely stabilizes their active open conformation and therefore their interaction with agonist-activated receptors during the early steps of endocytosis.

The IVF motif was initially characterized for its function in the control of the activation state of the molecule (14,15,19). Here, we demonstrate that it also plays a previously unappreciated central and dual role in AP-2 binding. Whereas the F residue is directly involved in the interaction with the β2-adaptin ear platform domain [(18,25) and therein], the I and the V seem to negatively control the affinity of the adjacent downstream peptide for the ear domain of β2-adaptin. Two different mechanisms could account for the observed increased AP-2 binding efficiency upon mutation of I and V residues. The V is pointing laterally on the side of the βarr α-helix, making contact with the top of the α-helix of the β2 ear platform (Figure 9), thus likely impeding the βarr peptide to enter deeply into the β2 ear groove. Accordingly, the observed increased AP-2 binding efficiency upon alanine substitution of the V residue could be explained by a greater insertion of the βarr peptide into the β2 ear groove. The I residue is found on the top of the α-helix formed by the βarr peptide, and it does not establish any contact with the β2-adaptin ear (Figure 9). It might negatively regulate the transition of the βarr peptide from the extended conformation to the α-helix, consistent with the fivefold increased affinity for AP-2 observed with the peptide, in which the I residue is substituted by an alanine. A direct role in the control of the α-helix transition could also explain the effect of the I to A mutation in the constitutive 'opening' of full-length βarr, as the transition to the α-helix is also expected to favor the release of the βarr C-tail from its intramolecular interaction with the globular domains. Finally, the observation that alanine substitutions of I and/or V residues markedly enhanced the affinity of the peptide for AP-2, suggests that these residues negatively regulate this interaction and therefore allow an optimal equilibrium between the closed inactive and AP-2-bound conformations of βarrs.

Whatever the mechanism involved, mutations of both the I and the V of the IVF motif (AAF mutant) allowed us to generate a βarr mutant in the active open conformation, which is constitutively targeted into CCPs, and constitutes a novel tool to investigate βarr function. Indeed, the previously characterized mutants of the IVF motif consisted in a triple alanine mutation (3A), which resulted in a constitutively active form of βarr (14) but also affected in its ability to bind to AP-2 because of mutation of the F residue [Figure 3, (18,25)]. As a proof of the relevance of the AAF mutant as a constitutively active open form of βarr, our results show that its accumulation in CCPs reached the maximal level observed for wild-type protein upon 'physiological' stimulation by agonist (Figure 7). These data are also in agreement with the observation that the AAF mutant showed a similar capacity to wild-type protein to stimulate internalization of agonist-activated GPCR, likely because of its inability to recruit more activated GPCR per CCP than wild-type molecule physiologically activated by GPCR stimulation. Altogether, these observations strongly support the concept that the AAF mutant mimics a constitutively active open form of βarr.

The fact that the AAF mutant of βarr is targeted to CCPs in the absence of receptor activation, indicates that binding to phosphorylated agonist-activated GPCRs is not strictly required for CCP targeting and that βarr accumulation in CCPs mostly relies on the release of a targeting signal, which corresponds to both AP-2 and clathrin-binding sites of the C-terminal tail (Figures 2 and 7). In a similar manner, the previously reported binding of βarrs to plasma membrane phosphoinositides (40) is probably not directly required for CCP targeting. It is rather likely involved in full

Figure 8: Dynamic analysis of the AAF activated mutant shows is absence in forming CCVs. A and B) HeLa cells transiently transfected with a GFP-tagged βarr2 AAF mutant construct were analyzed by confocal microscopy. A focal plane containing the adherent surface of the cells was used for all analyses. A small region of the cell was photobleached and recovery of fluorescence was followed (one image every 1.6 seconds) (A). The recovery of fluorescence was quantified by measuring the fluorescence intensity of GFP inside the photobleached region over time. Values were normalized with the fluorescence intensity measured in a nonbleached region (B; $n = 5$). C–F) HeLa cells were transiently transfected with both GFP-tagged βarr2 AAF mutant and DsRed-tagged clathrin light chain constructs and analyzed the day after transfection by live cell TIR-FM imaging. The AAF mutant was absent from the subpopulation of CS, which disappear from the evanescent field (D). The absence of AAF mutant in a disappearing CS was quantified (E) by measuring fluorescence normalized to local background for GFP (βarr2) and DsRed (clathrin) inside the disappearing CS stressed by an arrow in D. The same operation was repeated for the indicated number of spots of each category to calculate the mean normalized fluorescence intensity of AAF mutant in static and disappearing CS (F).

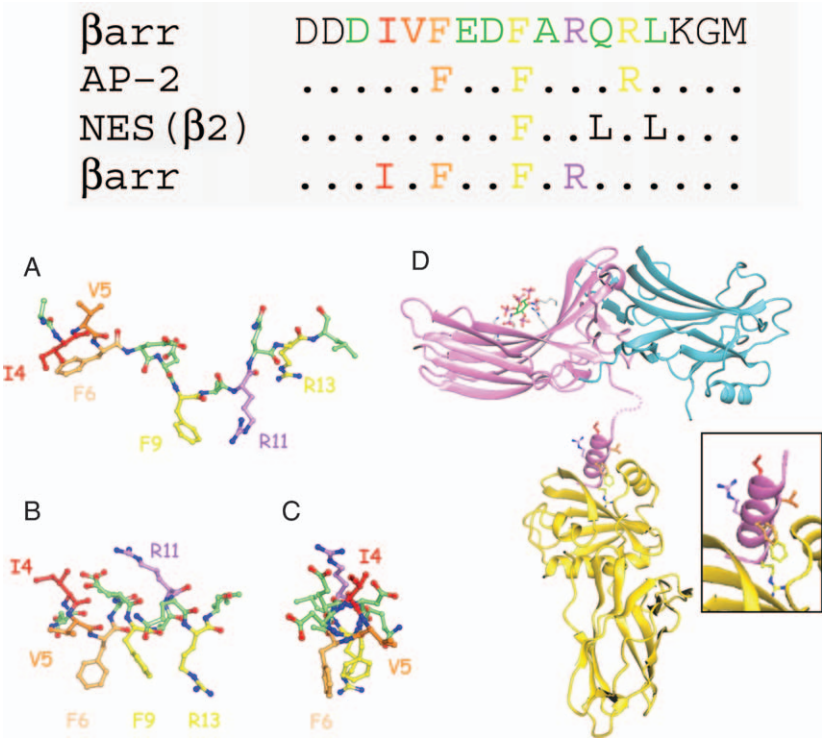

Figure 9: Structure–function analysis of the AP-2 binding region of the C-terminal tail of βarr. Residues of the C-terminal tail of βarr are labeled with the same color code as in Figure 1 (red to orange: IVF, yellow: AP-2 binding, purple: R393 and bold black: NES of βarr2). The residues involved in intramolecular interaction (βarr), AP-2 binding (AP-2) and nuclear export (NES, in the case of βarr2) are indicated. A) Structure of the corresponding peptide in native βarr1. B and C) Structure of the same peptide solved from the complex with the ear domain of β2-adaptin. The helix is shown in two different views (B and C) to help visualizing the orientation of the IVF residues. D) Model for βarr/β2 ear complex.

activation of endocytic functions of βarrs once they are recruited to the plasma membrane. A similar mechanism has been proposed for the μ2 subunit of the AP-2 complex, which binds more efficiently to internalization signals and is stabilized in an open conformation upon phosphoinositides binding (41). Although the AAF mutant of βarr was fully competent to recruit ligand-activated TRH-R in CCPs (Figure 7) and then in endosomes (Figure S5), it was excluded from forming CCV (i.e., dynamic spots in TIR-FM) and endosomes (data not shown) in the absence of receptor activation. These observations indicate a previously unappreciated active role of the cargo in the translocation of receptor-βarr complex into forming CCV, this function being so far attributed to βarrs.

Finally, all the above results reveal a striking accumulation of three distinct functional domains within a short 15 amino acid residue region of the C-terminal tail of βarrs (Figure 9). Indeed, this region includes (i) the IVF motif, which participates in the docking of the C-terminal tail onto the N-terminal domain in the close conformation and directly participates in the interaction with the β2-adaptin ear domain (F6) in the open conformation; (ii) residues directly involved in AP-2 binding (F6, F9 and R13); (iii) in the case of βarr2, residues required for NES activity (F9, L12 and L14). In addition, earlier work by V. Gurevich and collaborators indicated that mutations of two residues in the C-tail of visual arrestin, corresponding to F9 and R11 of the βarr peptide, resulted in constitutively active phenotypes (19). The R11 is likely to play a crucial role in maintaining the closed inactive conformation of arrestins because it interacts with residues belonging to both N- and C-terminal globular domains (Figure 1C), and therefore it might maintain the association of the two globular domains. The direct role of R11 in AP-2 binding has remained controversial so far (12,16). The fact that this residue resides on the top of the βarr α-helix (Figure 9B,C) supports the hypothesis that it is not directly involved in the interaction with AP-2. However, the fact that the I4 of the IVF motif is also found on the top of the helix and that its mutation into alanine indeed affects AP-2 binding indicates that the presence of a residue on top of the helix does not necessarily mean that its mutation will not affect β2 ear domain binding.

Among all the residues of this 15 amino acid region, the F9 appears to be the most critical because it is involved in three distinct functions, including intramolecular interaction, interaction with AP-2 and nuclear export activity. Although, the solved structures of native βarr and of the βarr peptide complexed to AP-2 provides a clear indication of how F9 may be involved in stabilizing the resting state of βarrs and in their interaction with AP-2 (see above), it remains to be determined, from a mechanistic point of view, how it could be involved in the the nuclear export of βarr2 (22). In the two conformations of the βarr C-tail (closed inactive and open interacting with AP-2), F9 appears completely buried and not accessible to other interactions. Its direct role in regulating nuclear export, however, suggests that it might be accessible to the exportin Crm1, which controls nuclear export through direct binding to NES (42),

and accordingly that βarr2 might be found in the nucleus in the active conformation.

Materials and Methods

Plasmids

The GFP-tagged constructs derived from rat βarr2, including wild type, R396A (AP-2-binding mutant) and I387A (AVF) point mutants, and the C-terminal tail fragments C1 (317–410), C5 (317–400) and C6 (317–390) were described previously, together with the C1 fragment (315–418) from human βarr1 (21). The GFP-tagged rat βarr2 mutant deficient for clathrin binding (AAEA) was a kind gift of Marc Caron (Duke University Medical Center, Durham, NC, USA). The point mutants of the IVF motif including V388A (IAF), F389A (IVA), I387A/V388A (AAF) and I387A/V388A/F389A (3A) were generated, as described in (19). The sequences of the mutagenic primers are available on request. A plasmid coding for wild-type βarr2 fused to GFP (EGFP-N1, Clontech, BD Biosciences, Le-Pont-de-Claix, France) was used as template. Double mutants deficient for clathrin binding (AAEA-R396A and AAEA-AAF) were generated using a plasmid coding for the AAEA βarr2 mutant as template. To introduce the same mutations in the C-terminal tail context, the corresponding region was amplified by polymerase chain reaction (PCR) using the relevant point mutant encoding plasmids as template. The PCR products were subcloned into the pCR3.1 vector using the Eukaryotic TA Expression Kit from Invitrogen (Cergy Pontoise, France). To generate the corresponding GFP and GST fusion proteins, the fragments were subcloned from PCR3.1 into pEGFP-C2 (Clontech, BD Biosciences) and pGEX-5-X1 (GE Healthcare, Saclay, France) vectors using the appropriate restriction sites present in PCR primers. GST fusion constructs of wild-type βarr2 and IVF motif mutants were generated by transferring βarr2 fragments from GFP vectors into pGEX-5-X1 vector. All the above constructs were verified by nucleotide sequencing (Sequencing facility of the Cochin Institute).

Myc and 6xHis-tagged human-β2-adaptin ear domain (700–937) constructs were described previously (43). Clathrin–DsRed (light chain), Caveolin1-mRFP and VSV-tagged TRH-R constructs were kind gifts from T. Kirchhausen (Harvard Medical School, CBR Institute for Biomedical Research, Boston, MA, USA), R. Pagano (Mayo Clinic College of Medicine, Rochester, MN, USA) and G. Milligan (University of Glasgow, Glasgow, UK), respectively.

Cells, transfection, antibodies and reagents

HeLa cells were grown in DMEM supplemented by 10% fetal bovine serum (Invitrogen). Cells were transiently transfected using either the Calcium Phosphate Kit from Invitrogen, Genejuice from Novagen (VWR, Fontenay sous bois, France) or Fugene6 from Roche Diagnostic (Indianapolis, IN, USA) according to the manufacturers' instructions. Rabbit polyclonal antibody M-300 and mouse monoclonal 100/2 against the α-adaptin subunit of AP-2 were from Santa Cruz (Tebu-bio, Le Perray en Yvelines) and Sigma (St Quentin Fallavier, France), respectively. Mouse monoclonal anti-myc (9E10) was from Roche Diagnostics. Alexa633-labeled goat anti-rabbit, Alexa594-labeled goat anti-mouse, goat anti-rabbit and Alexa647-labeled transferrin were from Molecular Probes (Invitrogen). Cy3-labeled anti-VSV antibody (P5D4), TRH and Leptomycin B were from Sigma. Cy5-labeled donkey anti-rabbit secondary antibody was from Jackson ImmunoResearch (Interchim, Montlucon, France). Tritium-labeled human TRH ($^{[3H]}$TRH) was from Perkin Elmer (Courtaboeuf, France).

Internalization assay

Internalization of radioactive TRH was measured as previously described (21) with minor modifications. Briefly, COS cells were seeded in 12-well plates (80 000 cells/well). The day after cells were transfected with both TRH-R and GFP or GFP-tagged encoding plasmids. Forty-eight hours later, DMEM was removed from the cells and replaced with 0.5 mL HEPES-buffered (HB) medium (serum free DMEM, 20 mM HEPES, pH 7.2) per well, and cells were incubated at 37 °C. Forty minutes later, plates were placed on ice and cooled for 10 minutes. HB medium was removed and replaced with 200 μL of 50 nM $^{[3H]}$TRH in HB medium, and cells were incubated on ice for 40 minutes. Subsequently, plates were shifted to 37 °C for 10 minutes, replaced on ice and washed three times with ice cold 0.15 M NaCl. Immediately after, membrane-bound $^{[3H]}$TRH was stripped with 0.5 mL of an acid/salt wash (0.2 M acetic acid, 0.5 M NaCl, pH 2.6) followed by 0.5 mL of 0.15 M NaCl wash. Internal $^{[3H]}$TRH was determined following cell solubilization with 1% (w/v) SDS/1% (v/v) triton-X-100/10 mM Tris/HCl, pH 8.0. Cells transfected with pcDNA3.1 empty control vector were used to calculate non-specific binding. Results are expressed as a percentage of surface receptors internalized at 10 minutes.

Immunofluorescence

HeLa cells were grown on coverslips and used for immunofluorescence studies the day after transfection. Cells were washed in PBS and fixed in 3.7% paraformaldehyde 0.03 M sucrose for 30 minutes at 4 °C, then washed once in PBS and quenched in 50 mM NH4Cl in PBS. The cells were then incubated with primary antibodies in permeabilization buffer (PBS supplemented with 1 mg/mL BSA and 0.1% triton-X-100) for 45 minutes at room temperature. After two washes with PBS 1 mg/mL BSA, cells were incubated for 45 minutes at room temperature in PBS 1 mg/mL BSA containing secondary antibodies. After two washes in permeabilization buffer and one in PBS, the cells were mounted on microscope slides in PBS–glycerol (50/50) using the SlowFade Light Antifade Kit with DAPI from Molecular Probes (Invitrogen). Stimulation of transfected cells with TRH was done as previously described (28). Briefly, HeLa cells cotransfected with GFP-tagged βarr2 fusions and VSV-tagged TRH-R were first incubated for 1 h at 4 °C with Cy3-labeled anti-VSV antibody. Cells were washed and then either fixed immediately or after incubation for the indicated time in the presence of TRH alone or with TRH and Alexa647-labeled transferrin. Cells were finally washed again in cold media, then fixed and processed for immunofluorescence as described above.

Samples were examined under an epifluorescence microscope (Leica, Reuil Malmaison, France) with a cooled charge-coupled device (CCD) camera (Micromax, Roper Scientific, Evry, France). Images were acquired with MetaMorph (Universal Imaging, Downingtown, PA, USA) and processed with MetaMorph, National Institutes of Health (NIH) image (rsb.info.nih.gov/nih-image/) and Photoshop (Adobe Systems Inc., San Jose, CA, USA).

Live cell imaging

For dynamic analysis of βarr2 mutant at the plasma membrane, total internal reflection fluorescence microscopy (TIR-FM) was performed as described (39) using an Apo 60X NA 1.45 microscope objective (Olympus, Olympus America Inc., Melville, NY, USA) with an inverted epifluorescence microscope (IX-70, Olympus) placed within a home-built temperature-controlled enclosure set at 37 °C for live cell imaging. To image simultaneously both clathrin–DsRed and βarr-GFP fusions, both fluorophores were excited with the 488-nm line of the same tunable argon laser (Omnichrome, model 543-AP A01, Melles Griot, Carlsbad, CA, USA) reflected off the 498dclp dichroic mirror. Image acquisition was performed using an emission splitter (DualView, Optical Insights Santa Fe, NM, USA) with the images focused simultaneously onto an ORCA ER cooled-CCD (Hamamatsu Photonics, Hamamatsu City, Japan). The GFP/DsRed emissions were collected simultaneously through an emission splitter equipped with dichroic mirrors to split the emission (550 dc, long-pass filter). The GFP emission was then collected through an emission band-pass filter (HQ515/30 nm) and the DsRed through an emission long-pass filter (580 nm). All mirrors and filters were obtained from Chroma Technologies Corp. (Brattleboro, VT, USA). Streams of 100–300 frames were acquired at ∼300 ms/frame. Shutters, filters and camera as well as acquisition were controlled by MetaMorph (Molecular Dynamics, Downingtown, PA, USA).

For FRAP experiments, Hela cells expressing AAF βarr2 mutant were analyzed using a laser scanning confocal microscope (TCS SP2 AOBS, Leica) after excitation with a 488-nm laser line from an argon laser. A defined region

of the adherent surface of cells expressing βarr2-GFP was exposed to 100% laser intensity for 0.5–1 second and recovery of fluorescence was analyzed for 1–2 minutes with an image for every 1.6 seconds.

The final images were generated using NIH image (http://rsb.info.nih.gov/nih-image/) or scion image (http://www.scioncorp.com) and Photoshop (Adobe Systems Inc.).

Image analysis using Metamorph

For live cell imaging, analysis was performed as previously described (39,44). Briefly, following the subtraction of extracellular background, 12-bit dual-color TIR-FM image streams were aligned using a journal written for MetaMorph (Universal Imaging). On the basis of controls using single fluorophores (39), green to red bleed-through corrections of 10% for βarr-GFP and clathrin–DsRed were employed. To calculate the mean normalized fluorescence of βarr-GFP inside clathrin–DsRed spots, individual CS were circled using MetaMorph. The resulting regions were transferred to the βarr images, and the fluorescence intensity corresponding to GFP inside these regions was measured; this represented the fluorescence intensity of βarr inside CS. To normalize these values to the local background, the regions were shifted on the clathrin images to select equivalent regions outside CS. Then, the resulting regions were transferred on the βarr images. The average of the value obtained for GFP fluorescence inside these shifted regions represents the background fluorescence of GFP outside CS. The fluorescence intensity of βarr-GFP inside CS was divided by the average of the fluorescence of GFP outside CS to obtain the mean normalized fluorescence intensity inside CS. This was then repeated for spots from each dynamic population of CS.

The quantification of endogenous AP-2 and Clathrin–DsRed fluorescence intensities in GFP-βarr spots was performed following a similar process (see above), using TIR-FM images of fixed cells expressing both GFP-tagged βarr mutant and DsRed-tagged clathrin, stained for endogenous AP-2. Then, βarr spots were circled using Metamorph, and these regions were used to quantify AP-2 and clathrin signals inside and outside βarr spots. To quantify the relative recruitment of βarr constructs into CCPs in resting conditions or upon TRH stimulation, βarr-associated fluorescence (wild type or mutants) into AP-2 spots was measured using epifluorescence images of fixed cells, expressing GFP-tagged βarr constructs alone or GFP-tagged βarr constructs and VSV-tagged TRH-R. After staining for endogenous AP-2, AP-2 spots were circled and these regions were used to quantify AP-2 and clathrin signals inside and outside βarr spots.

For FRAP experiments, the signal in the bleached region was normalized to the global fading of the sample during the analysis, which was directly measured in an unbleached region of the same cell. The results were then expressed as the percentage of recovery from the initial signal before bleaching.

GST production, GST pull-down assays and ITC

The full-length and C-terminal tail βarr2 fusion proteins and GST were produced in BL21Ai cells (Invitrogen). Briefly, upon induction by 1 mM isopropyl-D-thiogalactoside for 5 h at 30 °C, cells were lysed by sonication in cold PBS containing protease inhibitors (Sigma), and the lysate was incubated for 30 minutes at 4 °C with triton-X-100 (1%). The GST fusion proteins contained in the soluble fraction were bound to glutathione–Sepharose beads (GE Healthcare) by a 1-h incubation at 4 °C. After washes in cold PBS 1M NaCl, GST fusion-loaded beads were immediately used for interaction assays (GST pull downs). HeLa cells were lysed by incubation in lysis buffer (50 mM Tris HCl pH 7.6, 1 mM ethylenediaminetetraacetic acid, 150 mM NaCl, 1% triton, 10 mM protease inhibitor cocktail (Sigma; 10% glycerol) for 30 minutes at 4 °C. After centrifugation to eliminate cell debris and nuclei, lysates were incubated with GST fusion-loaded Sepharose beads overnight at 4 °C. Bound proteins were separated by polyacrylamide gel electrophoresis and transferred on polyvinylidene fluoride transfer membranes (PVDF, GE Healthcare) using the NuPage electrophoresis system (Invitrogen). Immunoblotting was performed using the 100/2 anti-AP-2 antibody. Blots were revealed using the ECL+ Detection Kit (GE Healthcare).

Binding of peptides to ear domain of β2-adaptin (6xHis-human-β2-appendage) was investigated by ITC (26) using a VP-ITC (MicroCal Inc., Northampton, MA, USA) as described elsewhere (27). Peptides were purchased at greater than 95% purity from the Institute of Biomolecular Sciences, University of Southampton, UK.

Molecular modeling

All structure figures of βarr1 [PDB ID 1ZSH (17)] and the C-terminal tail of βarr interacting with β2-adaptin ear domain [PDB ID 2IV8 (18)] were made using Aesop (M. Noble, University of Oxford, Oxford, U.K., personal communication) and SwissPDBViewer (http://www.expasy.org/spdbv). The peptide interaction map shown in Figure 1C was generated using the output from LIGPLOT (45) as a starting point.

Acknowledgments

The authors thank people from the 'sequencing' and 'imaging' facilities of the Cochin Institute; M. Caron, T. Kirchhausen, R. Pagano and G. Milligan for their kind gifts of βarr, clathrin, caveolin and TRH-R encoding plasmids; and Pierre Bourdoncle, Georges Bismuth and Anahi Molla for their help with FRAP analysis. This work was supported by grants from the 'Association pour la Recherche contre le Cancer (ARC)' (36–91, A. B.), NIH 1 F32 GM069200-02 (J. Z. R.), BES-0119468 (S. M. S.) and the Wellcome Trust and SIDACTION (M. G. H. S.).

Supplementary Materials

Figure S1: AP-2 binding is required for constitutive CCP targeting of the C-terminal tail of βarrs. Upper panel: Schematic representation of βarrs and C-terminal tail C1 fragments. Lower panel: Hela cells were transiently transfected with GFP-tagged constructs encoding for the wild-type C-terminal tail domains of either human βarr1 (residues 315–418; A) or rat βarr2 (C1: residues 317–410; B) or with mutants of rat βarr2 fragment C5 (C) and C6 (D). After fixation and permeabilization, cells were processed for immunofluorescence microscopy using an anti-AP-2 antibody and revealed by an Alexa594-labeled secondary antibody. The focus was made on the planar plasma membrane adherent to the coverslip to better visualize the localization of the constructs in CCPs. Insets show higher magnifications of representative areas. To help to visualize colocalizing of arrestin spots (GFP, green) AP-2 spots (Alexa594, red) were shifted from several pixels on the left.

Figure S2: CCP localization of IVF mutants. A) Hela cells were transiently transfected with GFP-tagged constructs corresponding to AVF (A and B), or IVA (C and D) mutants of the IVF motif in the full-length context. After fixation and permeabilization, cells were processed for fluorescence microscopy using the M-300 mouse anti-AP-2 antibody and revealed by an Alexa594-labeled secondary antibody. Insets show higher magnifications of representative areas and colocalizing spots are indicated by arrows. A and C) green fluorescence emitted by GFP (βarr2). B and D) red fluorescence emitted by Alexa594 (AP-2).

Figure S3: The AAF mutant does not localize to caveolae. Hela cells were transiently cotransfected with the A) GFP-tagged AAF mutant and B) mRFP-tagged caveolin1. Live cells were directly imaged by TIR-FM at 37 °C. C) overlay image. Inset shows higher magnification of a representative area. D) Quantification of GFP and mRFP fluorescence in spots corresponding to caveolin1 and AAF mutant, respectively. Fluorescence

intensity of each spot was normalized by substracting the background fluorescence intensity. E) The fluorescence intensities of GFP and mRFP were measured inside and outside caveolin1 and AAF mutant spots, respectively. The fluorescence inside spots is expressed as a percentage of the total fluorescence inside and outside the spot.

Figure S4: The AAF mutant constitutively shuttles in and out of the nucleus. Hela cells were transiently transfected with the GFP-tagged AAF mutant and treated (D–F) or not (A–C) with leptomycin B (LMB) for 45 minutes. Cells were then fixed and nuclei were stained with DAPI (C and F). Focus was made on the adherent surface of the cells (A and D) to show CCP localization or on a medial section of the cells (B, C, E and F) to show nuclear translocation upon leptomycin B treatment.

Figure S5: Activated mutants of βarr does not bypass agonist activation requirement for GPCR endocytosis. HeLa cells were transiently transfected with GFP-tagged wild type or AAF mutant of βarr2 together with a TRH-R construct with extracellular VSV tag. Cell surface TRH-R were stained with a Cy3-conjugated anti-VSV antibody at 4 °C and then either directly fixed or processed for immunofluorescence (A–D) or stimulated with TRH for 20 minutes in the presence of Alexa647-labeled transferrin (E–H). Cells were then washed and fixed directly observed by epifluorescence microscopy. A, C and E) green fluorescence emitted by GFP (βarr). B, D and F) red fluorescence emitted by Cy3 (TRH). G) Far red fluorescence emitted by Alexa647 (transferrin). H) Combined image from E, F and G.

Supplemental materials are available as part of the online article at http://www.blackwell-synergy.com

References

1. Lefkowitz RJ, Shenoy SK. Transduction of receptor signals by beta-arrestins. Science 2005;308:512–517.
2. Gurevich VV, Gurevich EV. The molecular acrobatics of arrestin activation. Trends Pharmacol Sci 2004;25:105–111.
3. Granzin J, Wilden U, Choe HW, Labahn J, Krafft B, Buldt G. X-ray crystal structure of arrestin from bovine rod outer segments. Nature 1998;391:918–921.
4. Hirsch JA, Schubert C, Gurevich VV, Sigler PB. The 2.8 A crystal structure of visual arrestin: a model for arrestin's regulation. Cell 1999;97:257–269.
5. Han M, Gurevich VV, Vishnivetskiy SA, Sigler PB, Schubert C. Crystal structure of beta-arrestin at 1.9 A: possible mechanism of receptor binding and membrane Translocation. Structure (Camb) 2001;9: 869–880.
6. Milano SK, Pace HC, Kim YM, Brenner C, Benovic JL. Scaffolding functions of arrestin-2 revealed by crystal structure and mutagenesis. Biochemistry 2002;41:3321–3328.
7. Lefkowitz RJ, Whalen EJ. Beta-arrestins: traffic cops of cell signaling. Curr Opin Cell Biol 2004;16:162–168.
8. Xiao K, Shenoy SK, Nobles K, Lefkowitz RJ. Activation-dependent conformational changes in {beta}-arrestin 2. J Biol Chem 2004;279: 55744–55753.
9. Hanson SM, Francis DJ, Vishnivetskiy SA, Kolobova EA, Hubbell WL, Klug CS, Gurevich VV. Differential interaction of spin-labeled arrestin with inactive and active phosphorhodopsin. Proc Natl Acad Sci U S A 2006;103:4900–4905.
10. Goodman OB Jr, Krupnick JG, Santini F, Gurevich VV, Penn RB, Gagnon AW, Keen JH, Benovic JL. Beta-arrestin acts as a clathrin adaptor in endocytosis of the beta2-adrenergic receptor. Nature 1996; 383:447–450.
11. Laporte SA, Oakley RH, Zhang J, Holt JA, Ferguson SS, Caron MG, Barak LS. The beta2-adrenergic receptor/betaarrestin complex recruits the clathrin adaptor AP-2 during endocytosis. Proc Natl Acad Sci U S A 1999;96:3712–3717.
12. Laporte SA, Oakley RH, Holt JA, Barak LS, Caron MG. The interaction of beta-arrestin with the AP-2 adaptor is required for the clustering of beta 2-adrenergic receptor into clathrin-coated pits. J Biol Chem 2000;275:23120–23126.
13. Celver J, Vishnivetskiy SA, Chavkin C, Gurevich VV. Conservation of the phosphate-sensitive elements in the arrestin family of proteins. J Biol Chem 2002;277:9043–9048.
14. Kovoor A, Celver J, Abdryashitov RI, Chavkin C, Gurevich VV. Targeted construction of phosphorylation-independent beta-arrestin mutants with constitutive activity in cells. J Biol Chem 1999;274:6831–6834.
15. Gurevich VV, Benovic JL. Mechanism of phosphorylation-recognition by visual arrestin and the transition of arrestin into a high affinity binding state. Mol Pharmacol 1997;51:161–169.
16. Kim YM, Benovic JL. Differential roles of arrestin-2 interaction with clathrin and adaptor protein 2 in G protein-coupled receptor trafficking. J Biol Chem 2002;277:30760–30768.
17. Milano SK, Kim YM, Stefano FP, Benovic JL, Brenner C. Nonvisual arrestin oligomerization and cellular localization are regulated by inositol hexakisphosphate binding. J Biol Chem 2006;281:9812–9823.
18. Schmid EM, Ford MG, Burtey A, Praefcke GJ, Peak-Chew SY, Mills IG, Benmerah A, McMahon HT. Role of the AP2 beta-Appendage Hub in Recruiting Partners for Clathrin-Coated Vesicle Assembly. PLoS Biol 2006:4e262.
19. Gurevich VV. The selectivity of visual arrestin for light-activated phosphorhodopsin is controlled by multiple nonredundant mechanisms. J Biol Chem 1998;273:15501–15506.
20. Vishnivetskiy SA, Schubert C, Climaco GC, Gurevich YV, Velez MG, Gurevich VV. An additional phosphate-binding element in arrestin molecule. Implications for the mechanism of arrestin activation. J Biol Chem 2000;275:41049–41057.
21. Scott MG, Le Rouzic E, Perianin A, Pierotti V, Enslen H, Benichou S, Marullo S, Benmerah A. Differential nucleocytoplasmic shuttling of beta-arrestins. Characterization of a leucine-rich nuclear export signal in beta-arrestin2. J Biol Chem 2002;277:37693–37701.
22. Wang P, Wu Y, Ge X, Ma L, Pei G. Subcellular localization of beta-arrestins is determined by their intact N domain and the nuclear export signal at the C terminus. J Biol Chem 2003;278:11648–11653.
23. Krupnick JG, Goodman OB Jr, Keen JH, Benovic JL. Arrestin/clathrin interaction. Localization of the clathrin binding domain of nonvisual arrestins to the carboxy terminus. J Biol Chem 1997;272:15011–15016.
24. Krupnick JG, Santini F, Gagnon AW, Keen JH, Benovic JL. Modulation of the arrestin-clathrin interaction in cells. Characterization of beta-arrestin dominant-negative mutants. J Biol Chem 1997;272:32507–32512.
25. Edeling MA, Mishra SK, Keyel PA, Steinhauser AL, Collins BM, Roth R, Heuser JE, Owen DJ, Traub LM. Molecular switches involving the AP-2 beta2 appendage regulate endocytic cargo selection and clathrin coat assembly. Dev Cell 2006;10:329–342.
26. Wiseman T, Williston S, Brandts JF, Lin LN. Rapid measurement of binding constants and heats of binding using a new titration calorimeter. Anal Biochem 1989;179:131–137.
27. Praefcke GJ, Ford MG, Schmid EM, Olesen LE, Gallop JL, Peak-Chew SY, Vallis Y, Babu MM, Mills IG, McMahon HT. Evolving nature of the AP2 alpha-appendage hub during clathrin-coated vesicle endocytosis. Embo J 2004;23:4371–4383.
28. Scott MG, Benmerah A, Muntaner O, Marullo S. Recruitment of activated G protein-coupled receptors to pre-existing clathrin-coated pits in living cells. J Biol Chem 2002;277:3552–3559.
29. Steyer JA, Almers W. A real-time view of life within 100 nm of the plasma membrane. Nat Rev Mol Cell Biol 2001;2:268–275.

30. Rappoport J, Simon S, Benmerah A. Understanding living clathrin-coated pits. Traffic 2004;5:327–337.
31. Perrais D, Merrifield CJ. Dynamics of endocytic vesicle creation. Dev Cell 2005;9:581–592.
32. Kudo N, Matsumori N, Taoka H, Fujiwara D, Schreiner EP, Wolff B, Yoshida M, Horinouchi S. Leptomycin B inactivates CRM1/exportin 1 by covalent modification at a cysteine residue in the central conserved region. Proc Natl Acad Sci U S A 1999;96:9112–9117.
33. Santini F, Gaidarov I, Keen JH. G protein-coupled receptor/arrestin3 modulation of the endocytic machinery. J Cell Biol 2002;156: 665–676.
34. Ashworth R, Yu R, Nelson EJ, Dermer S, Gershengorn MC, Hinkle PM. Visualization of the thyrotropin-releasing hormone receptor and its ligand during endocytosis and recycling. Proc Natl Acad Sci U S A 1995;92:512–516.
35. Oakley RH, Laporte SA, Holt JA, Caron MG, Barak LS. Differential affinities of visual arrestin, beta arrestin1, and beta arrestin2 for G protein-coupled receptors delineate two major classes of receptors. J Biol Chem 2000;275:17201–17210.
36. Wu X, Zhao X, Baylor L, Kaushal S, Eisenberg E, Greene LE. Clathrin exchange during clathrin-mediated endocytosis. J Cell Biol 2001;155: 291–300.
37. Wu X, Zhao X, Puertollano R, Bonifacino JS, Eisenberg E, Greene LE. Adaptor and clathrin exchange at the plasma membrane and trans-Golgi network. Mol Biol Cell 2003;14:516–528.
38. Rappoport JZ, Taha BW, Lemeer S, Benmerah A, Simon SM. The AP-2 complex is excluded from the dynamic population of plasma membrane-associated clathrin. J Biol Chem 2003;278:47357–47360.
39. Rappoport JZ, Benmerah A, Simon SM. Analysis of the AP-2 adaptor complex and cargo during clathrin-mediated endocytosis. Traffic 2005; 6:539–547.
40. Gaidarov I, Krupnick JG, Falck JR, Benovic JL, Keen JH. Arrestin function in G protein-coupled receptor endocytosis requires phosphoinositide binding. Embo J 1999;18:871–881.
41. Honing S, Ricotta D, Krauss M, Spate K, Spolaore B, Motley A, Robinson M, Robinson C, Haucke V, Owen DJ. Phosphatidylinositol-(4, 5)-bisphosphate regulates sorting signal recognition by the clathrin-associated adaptor complex AP2. Mol Cell 2005;18:519–531.
42. Gorlich D, Kutay U. Transport between the cell nucleus and the cytoplasm. Annu Rev Cell Dev Biol 1999;15:607–660.
43. Owen DJ, Vallis Y, Pearse BM, McMahon HT, Evans PR. The structure and function of the beta 2-adaptin appendage domain. Embo J 2000; 19:4216–4227.
44. Burtey A, Rappoport JZ, Bouchet J, Basmaciogullari S, Guatelli J, Simon SM, Benichou S, Benmerah A. Dynamic interaction of HIV-1 Nef with the clathrin-mediated endocytic pathway at the plasma membrane. Traffic 2007;8:61–76.
45. Wallace AC, Laskowski RA, Thornton JM. LIGPLOT: a program to generate schematic diagrams of protein-ligand interactions. Protein Eng 1995;8:127–34.